Scientia Iranica (2024) 31(16), 1359–1373

Sharif University of Technology
Scientia Iranica
Transactions B: Mechanical Engineering
https://scientiairanica.sharif.edu

Numerical simulation of electroosmotic flow in a rectangular microchannel with use of magnetic and electric fields

Mohsen Saghafian*, Hossein Seyedzadeh, and Abolfazl Moradmand

Department of Mechanical Engineering, Isfahan University of Technology, Isfahan, 8415683111, Iran.

Received 5 June 2021; received in revised form 27 February 2023; accepted 25 June 2023

KEYWORDS
Aspect ratio;
Critical Hartmann number;
Debye Hückel;
Electric double layer;
Electrokinetic;
Electroosmotic flow;
Joule heating;
Magnetohydrodynamics;
Poisson-Boltzmann.

Abstract. Pumping fluid is one of the crucial parts of any microfluidic system. Using electric and magnetic fields as a substitute for moving parts can have many advantages. In this study hydrodynamic and heat transfer characteristics of electroosmotic flow under influence of lateral electric and transverse magnetic field, are studied numerically. Results indicate that the dimensionless parameters such as Hartmann number, intensity of the lateral electric field, pressure gradient parameter and aspect ratio have an important role in controlling flow. It can be implied that the enhancement of pressure gradient leads to the decrease of critical Hartmann number, and this dependency can be reduced from 44% to 7% for $S = 0.5$ to $S = 50$ in two pressure gradients of $\Omega = 1$ and $\Omega = 20$. In addition, the reduction of aspect ratio of microchannel section leads to the increment of critical Hartmann number in a specified lateral electric field. At the end, thermal analysis is being done by consideration of the effects of magnetic and electric fields on the Nusselt number.

1. Introduction

Microfluidics and Micro-Electro-Mechanical Systems (MEMS) have various applications such as heat exchangers, micro-pumps, separation machines, etc. [1–3]. The flow pumping part has been especially considered due to flow transfers to the different parts of fluidic system. In general, micro-pumps are divided into mechanical and non-mechanical groups. Due to the complexities of construction of moving parts and high pressure drop in the micro scale, mechanical fluid transfer is being involved with limitations, hence, transport mechanism has been used without moving parts [4]. There are different methods to transfer fluid inside the narrow channels such as applying pressure gradients, capillary effect and electric or magnetic fields [5–7]. Therefore, in recent decades, researchers have shown the potential of using the combination of electrokinetic and magnetohydrodynamics (MHD) in order to achieve the ideal flow control in devices with different shapes. Due to mechanical pumping issues in engineering applications such high power requirements,

*. *Corresponding author.*
E-mail addresses: saghafian@iut.ac.com (M. Saghafian); s.seyedzadeh@alumni.iut.ac.ir (H. Seyedzadeh); abolfazlmoradmand1@gmail.com (A. Moradmand)

To cite this article:
M. Saghafian, H. Seyedzadeh, and A. Moradmand "Numerical simulation of electroosmotic flow in a rectangular microchannel with use of magnetic and electric fields", *Scientia Iranica* (2024), **31**(16), pp. 1359–1373
https://doi.org/10.24200/sci.2023.58474.5742

friction loss, etc., the aforementioned techniques are crucial for stimulating fluids in modern industries. In the meantime, fluid flow and heat transfer are considered in the narrow channels.

Transport phenomenon has distinctive characteristics in the micro scale compared to macro scale which is due to the surface effects such as Electric Double Layer (EDL) [8]. The EDL is created due to the interaction of the ionized solution with free charge on the dielectric surfaces. Due to the electric field, mobile ions move in the EDL regions leading to transport of bulk liquid with viscose effects. This concept is called Electro-Osmotic Flow (EOF) [9]. Jang and Lee [4] were the first researchers who investigated micro pumps by using the driving force of MHD flow (Lorentz force), analytically and experimentally. They reported the amount of pressure difference and flow rate in a special condition. Wang et al. [10] numerically simulated 2-D, laminar and fully developed MHD flow inside a microchannel. They added Lorentz force as a source term to the momentum equation instead of analytical solution of Lorentz force due to applied magnetic field in momentum equation. Also, they revealed that induced Lorentz force has a significant effect on the flow velocity profile. Chakraborty and Paul [11] implemented Electro Magneto Hydrodynamic (EMHD) flow by considering pressure gradient inside a 2-D microchannel. They indicated that in the presence of specified lateral electric field with the aid of a relatively low-power magnetic field, the volumetric flow rate enhances. However, for high-intensity magnetic field and in the presence of lateral electric field, the volumetric flow rate decreases. Duwairi and Abdullah [12] studied heat transfer and MHD flow inside a rectangular micro-pump. They obtained velocity and temperature distribution analytically and numerically, then investigated the effects of different parameters on them. Chakraborty et al. [13] investigated heat transfer characteristics of a thermally fully developed EMHD flow between two parallel plates. They revealed that for a specific pressure gradient and axial electric field, the heat transfer characteristics in the micro scale can be significantly controlled by changing lateral electric and magnetic fields. Scandon et al. [14] analytically studied hydrodynamic and heat transfer characteristics of an EMHD and pressure-driven flow of a viscoelastic fluid inside a rectangular microchannel. Their results demonstrated that the volumetric flow rate enhances in the presence of electric and magnetic fields and also, this increment gives rise to the pressure gradient. In addition, the volumetric flow rate of Newtonian fluids is more sensitive to the MHD forces compared to viscoelastic fluids. Kiasatfar and Pourmahmoud [15] investigated flow and heat transfer of non-Newtonian conductive fluid inside a square microchannel under influence of a uniform magnetic field by using finite difference method. The obtained results revealed that increase in Hartmann number leads to a decrease in the maximum velocity of fluid and also, leads to the velocity profile's uniformity. Wang et al. [16] investigated EMHD flow of a non-Newtonian fluid between two parallel micro plates analytically and numerically by using perturbation techniques and compared the results with each other. They found out that by increasing Hartmann number, velocity and temperature decrease due to applied Lorentz force. Also, the augmentation of electric field intensity leads to the enhancement of velocity and temperature distributions in a specified Hartmann number. Sarkar et al. [9] studied the effect of non-uniform magnetic field on the mixed electroosmotic pressure-driven flow for thermally developed flow inside a fluidic narrow channel. They investigated flow, heat transfer and entropy generation and indicated that velocity and temperature distributions are symmetric when Hartmann number is non-zero. Qi and Wu [17] analytically implemented EMHD flow inside a rectangular microchannel under influence of the simultaneous magnetic and electric fields and obtained electric potential distribution. Also, they positioned the electric field as the deviant from the microchannel axis. Yang et al. [18] investigated fluid flow and heat transfer of EOF with the MHD effects inside a rectangular microchannel. They figured out that lateral electric field has a significant effect on the flow control and heat transfer and without the effect of lateral field, the normal velocity decreases gradually by increasing Hartmann number due to magnetic field's deterrent force. Moradmand et al. [19] numerically implemented Newtonian fluid's flow between two parallel micro plates, influenced by electric and magnetic fields. They concluded that in the electroosmotic flow, applying lateral electric field and transverse magnetic field causes creation of maximum possible flow rate for each Hartmann number and consequently, the increment of Hartmann number leads to reduction in flow velocity. Yang and Jian [20] studied a fully developed EMHD flow through the microchannel analytically and numerically. They used slip patterned boundary conditions with perturbation techniques under the assumption of small Reynolds number for analytical solution, and finite-difference method for numerical solution. Their results show that patterned slippage over the microchannel walls will induce a transverse flow which augments the mixing rate. Deng et al. [21] investigated the electroosmotic and pressure-driven flow of power-law fluids in a circular microchannel. The results show that both the viscosity and electroosmotic characters of inner power-law fluid, and the peripheral power-law fluid can affect the inner flow. Ge et al. [22] investigated the thermal resistance and pressure drop for the combination of Micro/mini-channel heat sinks, with rectangular rib,

by the multi-objective genetic algorithm and particle swarm optimization. Their results indicated that rib increases flow area, which results in transporting coolant flow in the secondary flow and consequently, heat transfer increment. Moreover, by changing shape from rectangular cross-section to curvy, pumping power reduced. Wang et al. [23] studied the flow mechanism and heat transfer increment of microchannel heat sinks with bi-direction ribs, numerically, and experimentally. Their results indicated that this design has better heat transfer, which is being concluded by significantly better Nusselt numbers. Biswas et al. [24] studied the thermal efficiency of a hybrid nano-fluid (Cu-Al_2O_3-H_2O) flow inside a porous oblique wavy cavity, with use of partly active magnetic field. Their results indicate that partially applied magnetic field on a complex wavy surface increase heat transfer significantly than the entire magnetic field. Mandal et al. [25] numerically studied the thermo-fluidic transport of a magnetic hydrodynamic mixture, including nanofluid, in a cavity with a wavy wall. They also used an Artificial Neural Network (ANN) method for statistical data. They considered the parameters influencing the flow for thermal evaluation. Their results revealed that heat transfer rate will increase for the curved-shape geometries. Moreover, they stated that ANN method can make an exact prediction for complicated shapes and Multiphysics geometries. Datta et al. [26] investigated heat transfer enhancement by studying three-dimensional transient conjugate heat transfer in microchannel heat sinks. They implemented different flow structures like combinations of ribs, cavities and protrusions on the side walls of a microchannel, and they used various geometric parameters like sidewall angles, number, and height of the top. Their results indicated that by changing the geometric parameters, they can control the heat transfer with them. Amit et al. [27] numerically studied the conjugate heat transfer for disruptive structures placed symmetrically in a rectangular microchannel. They used structures such as Triangular cavity, Secondary branch and Blockage to design a microsink. Their results indicate that cavity with secondary branch and blockage structure has the highest thermal performance and lowest entropy generation. So, the secondary branch can improve thermal performance of a microchannel with rectangular cavity. Biswas et al. [28] studied the free aspiration technique for heat transfer increment on MHD thermal convection and porous substances, by solving coupled mathematical equations of continuity, momentum, and energy. They used Maxwell model to utilize magnetic field and Brinkman-Forcheimer-Darcy model for porous media. Their results show that the free aspiration technique is able to remove heat from heat sources of the cavities, so it can increase heat transfer with no external pumping method. EMHD flow can be used in the bioconvection micropolar nanofluid, which is investigated in the work of Alharbi et al. [29]. The results of their work indicated the heat transfer rate of nanofluid, with use of self-similar variables. They also indicated that these parameters could control the flow and heat transfer.

Micropumps have many applications, especially in medicine delivery systems. One of the real applications of the current research's micropump is mentioned in the work of Ciocanel and Islam [30], which they manufactured an integrated EMHD micropump, which is a flow channel containing fluid to be pumped. They used electrodes and magnets to be responsible for electric and magnetic fields, which pump the fluid by a combination of electroosmotic and MHD flow. Also, this study has potential applications in biomedical devices. One specific real problem involving EOF with magnetic and electric fields is the development of microfluidic devices for biomedical applications, such as cell separation, manipulation in microfluidics, and drug delivery. For example, in a study published in the journal of magnetism and magnetic materials in 2021, researchers investigated the use of a magnetophoretic microfluidic chip with use of EOF, to separate Magnetic Particles (MPs) from human blood. Applying the magnetic field and electric potential makes a perfect on-chip separation, which is versatile for targeting magnetic particles [31].

Following a detailed review of the literature, many previous results pertain to 2D problems. But for practical applications, like drug targeting, cancer tumor treatment, devices for cell separation, endoscopy, and adjusting blood flow during surgery, it is imperative to provide a 3D solution. Moreover, to the best of our knowledge, the effect of the microchannel's geometry on the flow and critical Hartmann number has not been performed so far. Thus, the impact of microchannel geometry on the fluid flow and critical Hartmann number is investigated by considering different aspect ratios ($a = H/W = 0,\ 0.2,\ 0.5,\ 1,\ 2$). To model the electric potential distribution in the vicinity of walls, Poisson-Boltzmann equations with the linear Debye-Hückel approximation is used. The governing equations are discretized by applying the finite volume method and solved using a numerical code. In addition, for exact modeling, Joule heating is considered in the energy equation. The essential hydrodynamic and heat transfer parameters such as critical Hartmann number and Nusselt number are determined. The effect of different variables such as aspect ratio, the intensity of electric and magnetic fields on flow is studied.

2. Problem description

In the current research, fluid flow is studied inside a rectangular microchannel with the height of $2H$,

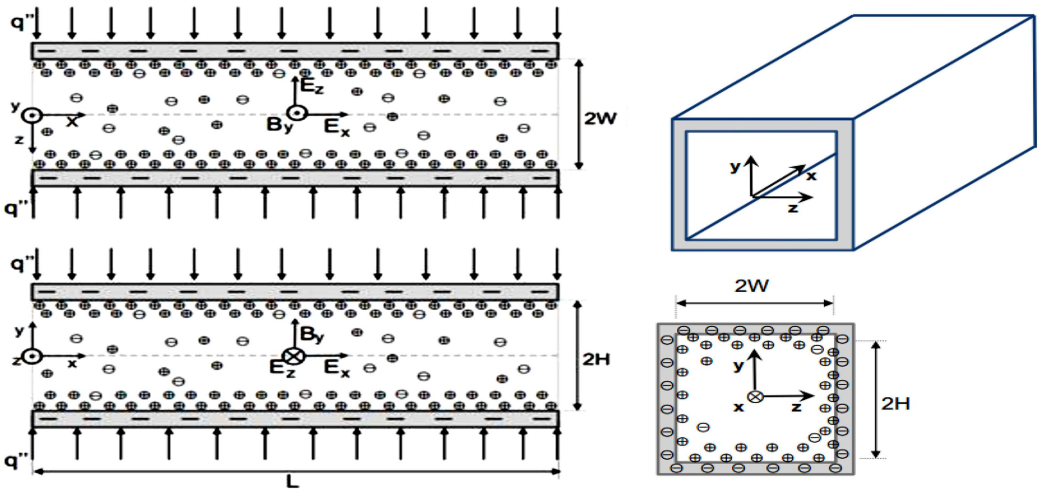

Figure 1. The geometry of microchannel.

width of $2W$ and length of L (according to Figure 1). The uniform axial and lateral electric fields (E_x and E_z) are applied along the x and z axes and also, the uniform transverse magnetic field (B_y) is applied along the y axis of microchannel. The coordinate axes are positioned such that the x axis is along the microchannel axis and there is the axial pressure gradient along it. The surface of microchannel is a dielectric surface when exposed to an electrolyte fluid, forms a layer called EDL. The Poisson-Boltzmann equation is used for modeling the ions in EDL.

3. Mathematical modeling

3.1. Electrokinetic equations

The charged walls of the channel create EDL in the vicinity of wall when exposed to the electrolyte solution. The electric potential distribution can be obtained by using Poisson equation [32]:

$$\nabla^2\psi = -\frac{\rho_e}{\varepsilon\varepsilon_0}, \tag{1}$$

when ε_0 is the permittivity of free space and ε_0 is the dielectric constant of electrolyte solution. The electric charge density ρ_e for symmetric electrolyte solution $z_+ = -z_-$ is [32]:

$$\rho_e = -2zen_0 \sinh\left(\frac{ze\psi}{k_BT}\right). \tag{2}$$

By combining Eqs. (1) and (2), the linearized Poisson-Boltzmann equation is obtained by applying Debye-Hückel approximation [32]:

$$\nabla^2\psi = \kappa^2\psi. \tag{3}$$

Consequently, by using Eq. (3), ψ is obtained and then by using obtained ψ and Poisson equation (Eq. (1)), ρ_e will be determined. Now, by computing electric charge density, the volumetric electrokinetic force or the force due to the electric field applied to fluid (electroosmotic force), can be obtained [32]:

$$\overrightarrow{F_{EK}} = \rho_e\overrightarrow{E}. \tag{4}$$

3.2. MHD equations

The force due to magnetic field (Lorentz force) is described as [33]:

$$\overrightarrow{F_B} = \overrightarrow{J}\times\overrightarrow{B}. \tag{5}$$

Magnetic field $\overrightarrow{B}$ includes an applied external field $\overrightarrow{B}_0$ and an inducted field $\overrightarrow{b}$. In micro scale flows, due to the low characteristic length and low average velocity, magnetic Reynolds number is low and consequently, the effect of induced magnetic field can be neglected against the applied external magnetic field. As a result, total magnetic field can be estimated by externally applied magnetic field [32,34]. J is induced electric current density [33]:

$$\overrightarrow{J} = \sigma\left(\overrightarrow{E} + \overrightarrow{U}\times\overrightarrow{B}\right). \tag{6}$$

3.3. Flow and energy equations under influence of electric and magnetic fields

According to the mentioned contents, volumetric force due to electric and magnetic fields is as follows [11]:

$$\overrightarrow{F} = \overrightarrow{F_{EK}} + \overrightarrow{F_B} = \rho_e\overrightarrow{E} + \overrightarrow{J}\times\overrightarrow{B}. \tag{7}$$

The assumptions considered are Newtonian fluid, steady state and incompressible flow. Also, pressure gradient is considered along the channel length. Heat flux is constantly applied to the side walls (up, down, right, left). Moreover, joule heating term is applied in the energy equation and viscous dissipation term is neglected. Therefore, the governing equations are as the following [13]:

$$\nabla.\overrightarrow{V} = 0, \tag{8}$$

$$\rho_f \left(\left(\overrightarrow{V}.\nabla \right) \overrightarrow{V} \right) = -\nabla P + \mu \nabla^2 \overrightarrow{V} + \overrightarrow{F}, \tag{9}$$

where, $\overrightarrow{V} = u\hat{i} + v\hat{j} + w\hat{k}$, ρ_f, P, μ, and $\overrightarrow{B}$ are velocity field, fluid density, pressure, fluid viscosity and volumetric force due to applied electric and magnetic fields on fluid, respectively. By applying the resultant force as a source term, momentum equation components will be as follows:

$$\rho_f \left(\left(\overrightarrow{V}.\nabla \right) u \right) = -\nabla P + \mu \nabla^2 u + \rho_e E_x - \sigma E_z B_y - \sigma u B_y^2, \tag{10}$$

$$\rho_f \left(\left(\overrightarrow{V}.\nabla \right) v \right) = -\nabla P + \mu \nabla^2 v, \tag{11}$$

$$\rho_f \left(\left(\overrightarrow{V}.\nabla \right) w \right) = -\nabla P + \mu \nabla^2 w + \rho_e E_z + \sigma E_x B_y - \sigma w B_y^2. \tag{12}$$

Energy equation [18]:

$$\rho_f C_P \left(\left(\overrightarrow{V}.\nabla \right) T \right) = k \nabla^2 T. \tag{13}$$

In Eq. (13), C_p is fluid's specific heat capacity in the constant pressure, T is temperature, k is conductivity coefficient and S_j is the generated heat in the volume unit of fluid due to the applied magnetic field to electrolyte solution (joule heating). By using Ohm's principle, joule heating phenomenon can be modeled as the heat source [7]:

$$S_j = \frac{\overrightarrow{J}^2}{\sigma}. \tag{14}$$

In Eq. (14), J and σ are electric current density and electrical conductivity of electrolyte solution, respectively. Also, joule heating can be obtained by using the values of electric and magnetic fields as follows:

$$S_j = \sigma \left[\left(\overrightarrow{E_x}^2 + \overrightarrow{E_z}^2 \right) + (wB_y)^2 + (uB_y)^2 - 2wE_xB_y + 2uE_zB_y \right]. \tag{15}$$

The boundary conditions of this study are presented in Table 1.

4. Numerical implementation

A numerical code based on the finite volume method is developed to solve momentum and energy equations (governing equations of fluid flow). The convection terms of governing equations in the integral form are discretized by using the QUICK method on a collocated grid. For pressure-velocity coupling, the pressure correction algorithm of SIMPLEC is applied. The Rai-Chow method is used to prevent nonphysical oscillations of pressure and velocity.

Table 1. Boundary conditions of the problem.

Inlet	Wall	Outlet
$u = u_{in}$	$u = 0$	Zero gradient in the direction perpendicular to outlet section
$v = 0$	$v = 0$	Zero gradient in the direction perpendicular to outlet section
$w = 0$	$q'' = -k\frac{\partial T}{\partial n}$	Zero gradient in the direction perpendicular to outlet section
$T = T_{in}$	$\psi = \zeta$	Zero gradient in the direction perpendicular to outlet section

After defining the physical properties of the system such as channel dimensions, properties of the fluid, applied electric and magnetic fields and discretizing the domain, the following procedures are applied for the present numerical simulation:

1. Solving the linearized Poisson-Boltzmann equation (Eq. (3)) to obtain electric potential distribution and then calculate the electric charge density from Poisson equation (Eq. (1));
2. Solving the Navier-Stokes equation using SIMPLEC algorithm (calculating and updating the velocity field based on the fluid properties and the applied fields);
3. Solving energy equation considering constant heat flux and Joule heating;
4. Iterating steps 1-3 until convergence.

The convergence criterion is the residuals in the continuity. The algorithm continues iterating until these criteria reach a desired level, such as when the residuals reduce by at least five orders of magnitude to a small value (such as 10^{-5}). This indicates that the solution has converged to an acceptable accuracy.

In this study, dimensionless parameters which are used for revealing the behavior of fluid are presented in Table 2. The values of the non-dimensional parameters taken into account for the following analysis reflect conditions that are practically realizable.

Table 2. Dimensionless parameters for implementing the results.

Dimensionless length	$(X,Y,Z)=\left(\frac{x}{D_H},\frac{y}{H},\frac{z}{W}\right)$	Dimensionless velocity	$(U,V,W)=\left(\frac{u}{U_{HS}},\frac{v}{U_{HS}},\frac{w}{U_{HS}}\right)$
Dimensionless average velocity	$U_m=\frac{u_m}{U_{HS}}$	Dimensionless temperature	$\theta=\frac{T-T_w}{T_m-T_w}$
Nusselt number	$Nu=\frac{hD_H}{k}$	Hartman number	$Ha=BD_H\sqrt{\frac{\sigma}{\mu}}$
Debye-Huckle parameter	$K=\kappa D_H=\sqrt{\frac{2e^2z^2n_0}{\varepsilon\varepsilon_0k_BT}}D_H$	Dimensionless axial electric field	$\alpha=\frac{E_xL}{\zeta}$
Dimensionless lateral electric field	$S=\frac{E_zD_H}{U_{HS}}\sqrt{\frac{\sigma}{\mu}}$	Dimensionless pressure gradient along the channel	$\Omega=\frac{\triangle PD_H^2}{\mu LU_{HS}}$
Dimensionless electric potential	$\Psi=\frac{ze\psi}{k_BT}$	Poiseuille number	$Po=C_fRe$
Reynolds number	$Re=\frac{\rho_f u_m D_H}{\mu}$		

Table 3. The percentage change for dimensionless temperature and Poiseuille number at $\alpha=2256$, $K=20$ and $\Omega=1$.

Grid	Percentage change of Po	Percentage change of θ
$a=0.5$, $S=0.25$, $Ha=0.25$		
$20\times32\times75$	1.53	0.4
$40\times64\times100$	1.53	0.4
$80\times128\times150$	–	–
$a=0$, $S=5$, $Ha=0.5$		
20×50	2.536	1.071
40×100	0.156	0.587
80×200	–	–
$a=1$, $S=1$, $Ha=0.5$		
$20\times20\times50$	2.434	0.896
$40\times40\times100$	0.326	0.896
$80\times80\times200$	–	–
$a=0.2$, $S=0.5$, $Ha=0.5$		
$16\times20\times75$	2.297	0.896
$32\times80\times100$	0.452	0.242
$64\times160\times150$	–	–

5. Validation of numerical solving procedure

5.1. Investigation of mesh independency

In the present investigation, some channels with various geometries are investigated. For each geometry, mesh independency is carried out separately in different values of electric and magnetic fields. The related results of Poiseuille number and dimensionless temperature are indicated in Table 3.

For a 3-D channel with a square cross-section, by increasing the grid from 40×40×100 to 80×80×200, the percentage of the change is less than 1%. Therefore, in this condition, a 40×40×100 grid is used as the primary grid for a microchannel with a square cross-section. For a 3-D microchannel with a rectangular cross-section, aspect ratios of $a=0.5$ and $a=0.2$ are considered. According to what was mentioned about square microchannel, in this condition, 40×64×100 and 32×80×100 grids are regarded as the main grids. For a 2-D microchannel ($a=0$), a 40×100 grid is proposed.

5.2. Validation

Validation of numerical code is investigated for a 3-D microchannel with square cross-section and 2-D microchannel, separately. To verify the accuracy of electric potential distribution in the vicinity of wall in the electrolyte solution, the study of Mirbozorgi et al. [35] is used. According to Figure 2, dimensionless electric potential distribution of this study is in agreement with the results of Mirbozorgi et al. with high accuracy.

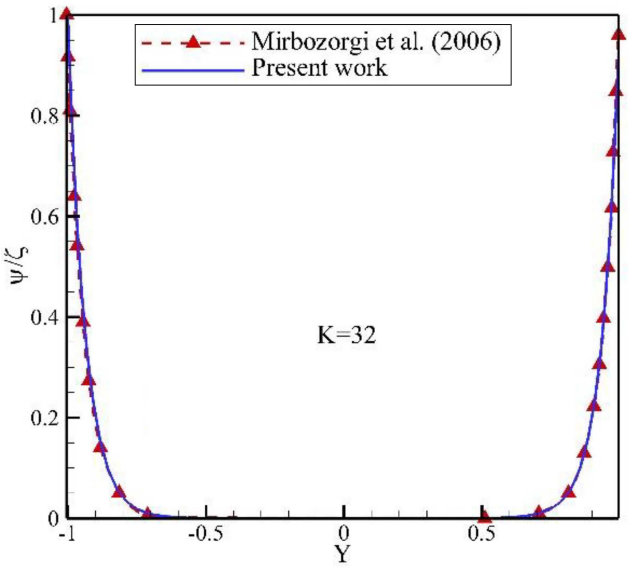

Figure 2. Dimensionless electric potential distribution in microchannel cross-section at $\zeta=-25$ mV and $K=32$.

Also, this accordance is seen in the vicinity of side wall region which has high potential variations.

For investigating the accuracy of numerical code of the fluid flow inside a square microchannel influenced by a transverse magnetic field and pressure gradient, study of Kiasatfar and Pourmahmoud [15] is used. According to Figure 3, this investigation has good agreement with the results of Kiasatfar and Pourmahmoud with the error of 1.3%.

In order to investigate the accuracy of numerical code in a pure EOF inside a square microchannel, study of Deng et al. [36] is utilized. According to Figure 4, for both values of dimensionless parameters of Debye-Hückel ($\kappa = 20$ and $\kappa = 100$) in all cross-sections,

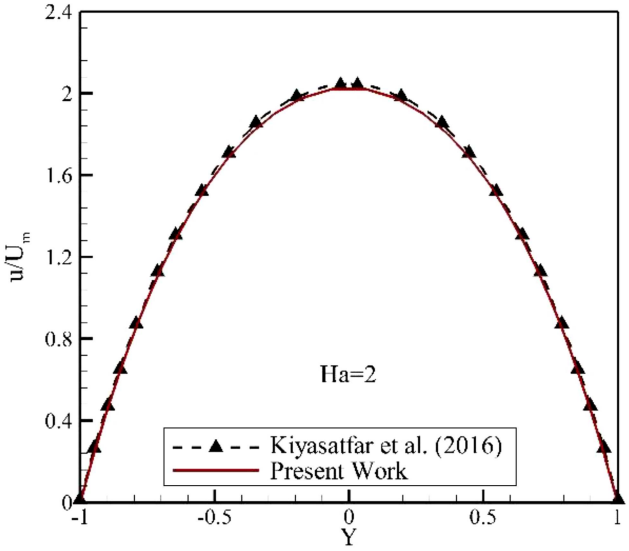

Figure 3. Velocity distribution under influence of $Ha = 2$.

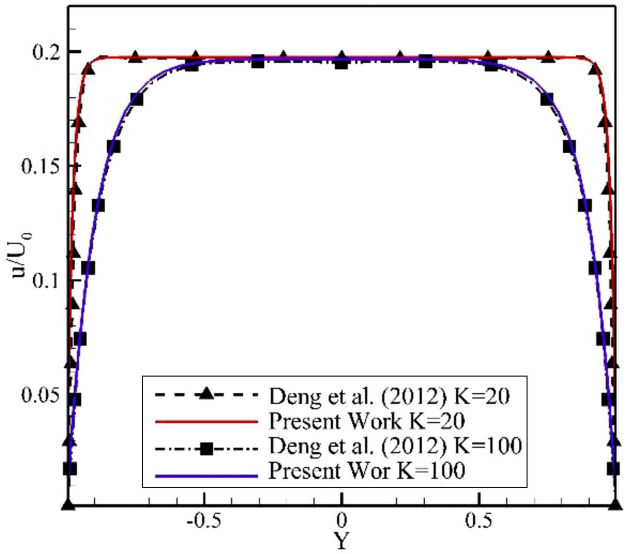

Figure 4. Velocity distribution diagram in square microchannel cross-section under influence of $E_x = 10000$ V/m in two values of $K = 20$ and $K = 100$.

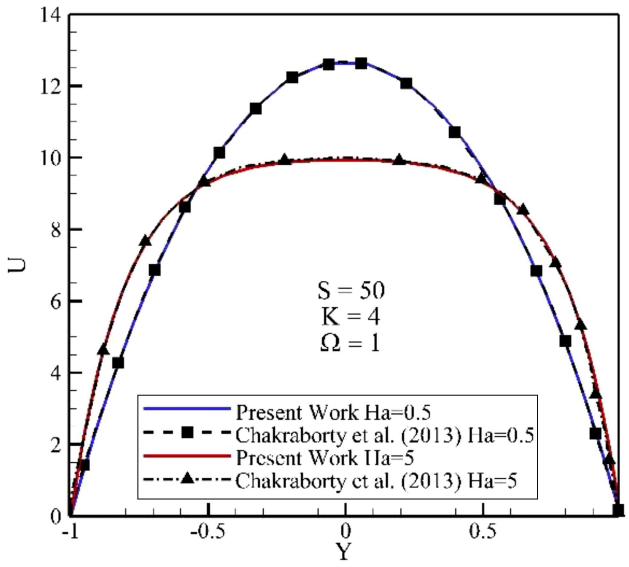

Figure 5. Velocity distribution in 2D microchannel cross-section under influence of $\alpha = 2256$, $S = 50$, $K = 4$, and $\Omega = 1$.

especially in the vicinity of wall, this research has acceptable concordance with that of Deng et al. [36]. Maximum difference is less than 1% in the case of $\kappa = 20$ and maximum variation is less than 0.25% in the case of $\kappa = 100$. It should be noted that for nondimensionalization of this profile, $U_0 = 0.001$ m/s is used [36]. Also, the effect of pressure gradient is not considered.

The study of Chakraborty et al. [13] is used for validation of a 2-D cross section microchannel. According to Figure 5, this research is in good accordance with the study of Chakraborty et al. [13] in all cross sections of microchannel, especially in the vicinity of wall.

6. Results and discussions

In this section, the flow and thermal characteristics are discussed by means of the non-dimensional parameters relevant to the present problem, which are presented in Table 2. The used ranges for these non-dimensionalized numbers are $Ha \sim 0.1{:}10$, $S \sim 0{:}100$, $\Omega \sim 1{:}20$, $a \sim 0{:}2$, which fall into practical values [37,38]. The values for α and κ are being selected as 2256 and 20.

6.1. Hydrodynamic investigation

Figure 6 indicates developed velocity profile of fluid flow inside a square cross section microchannel in the various values of Hartmann number (Ha) influenced by a dimensionless axial electric field (α) and dimensionless pressure gradient (Ω), by neglecting lateral electric field. As seen, by enhancing Ha, maximum velocity profile of passing flow decreases in microchannel's section due to the deterrent effect of magnetic field on fluid flow. Also, the simultaneous effects of deterrent force due to the transverse magnetic field and driving

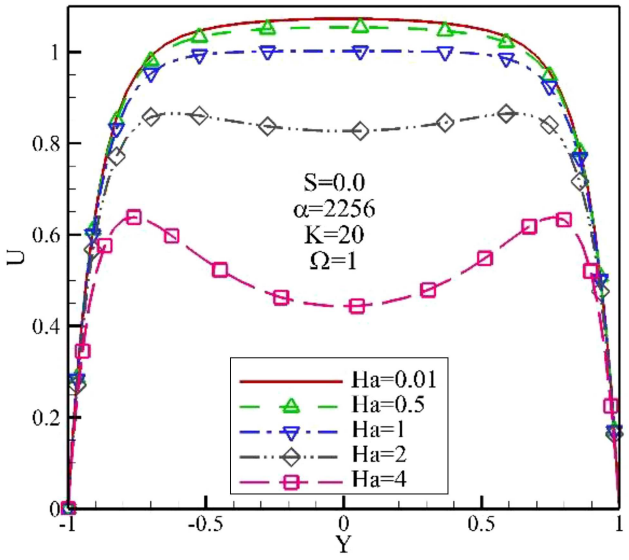

Figure 6. Velocity profile in microchannel with square cross-section under influence of $\alpha = 2256$, $Z = 0$, $K = 20$, and $\Omega = 1$ at different Hartmann numbers.

force due to the axial electric field cause concussion in the velocity profile at the high values of Ha.

In the pure EOF, the effect of axial electric field on microchannel leads to apply electrokinetic force on fluid flow. Also, applying transverse magnetic field leads to a reduction in maximum velocity in the microchannel's section. By affecting the lateral electric (E_z) and transverse magnetic (B_y) fields, the primary electric field (E_x), and fluid flow along the microchannel axis, secondary flow is created, seen by observing streamlines arrangement in microchannel cross-section. Basically, lateral electric and transverse magnetic fields interact with the charged particles in the fluid, inducing an electric current which generates a Lorentz force perpendicular to the axial field and flow direction. This force causes the fluid to move in a direction perpendicular to the primary flow. In Navier-Stokes equation along the z direction of Eq. (12), three extra source terms ($\rho_e E_z$, $\sigma E_x B_y$ and $\sigma w B_y^2$) are responsible for secondary flow. According to drawn streamlines in the contours of V and W velocity components of Figure 7, a flow is created opposite the Z-axis at the vicinity of walls along the Z-axis. Also, by colliding with the lower wall of microchannel, it deviated inward ($Y = 0$). Eventually, it causes two rotational flows in the microchannel's section.

Figure 8 demonstrates dimensionless velocity profile of developed EOF under influence of axial and lateral electric fields, with pressure gradient inside a 3-D square microchannel in different Hartmann numbers (Ha). By investigating the profiles, it can be concluded that for Ha less than 2, Ha augmentation leads to velocity enhancement. While, in Ha of greater than 2, increase in Ha results in velocity depletion. This phenomenon shows that if lateral electric field is applied to a microchannel, increment of transverse magnetic field to a specific value can increase maximum velocity in microchannel's section. After this particular value, increment of Ha leads to a decrease in maximum velocity in microchannel. This specific value is known as critical Hartmann number (Ha_{cr}) causing maximum flow rate in microchannel. In this case, Ha of 2 is equal to the Ha_{cr} [19]. Critical Hartmann number depends on the dimensionless parameter of lateral electric field (S). Therefore, its value can be obtained in each value of S.

Figure 9 represents average velocity as the function of Ha for $S = 0.75$ and $S = 5$. As seen, the Ha_{cr} is obtained as 0.372 for $S = 0.75$ and 2.061 for $S = 5$. The reason for the maximum flow rate for each specific magnetic field intensity (Ha_{cr}) in the presence of lateral electric field, can be found out by investigating added terms to the Navier-Stokes equation along the x direction ($-\sigma E_z B_y$ &$-\sigma u B_y^2$). By enhancing the value of transverse magnetic field, when driving part ($-\sigma E_z B_y$) is greater than deterrent part

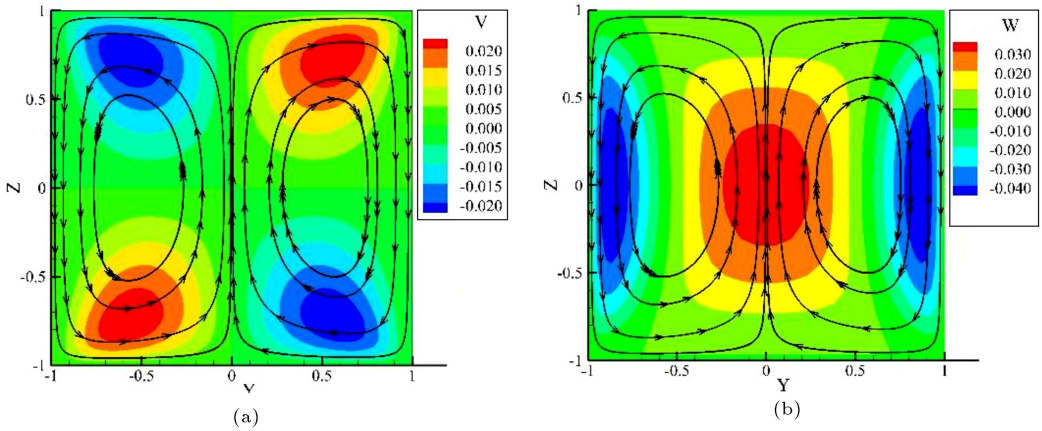

Figure 7. Streamlines of fluid flow in microchannel cross-section under influence of $S = 5$, $Ha = 0.5$, $\alpha = 2256$, $K = 20$, and $\Omega = 1$ on velocity contour (a) V component and (b) W component.

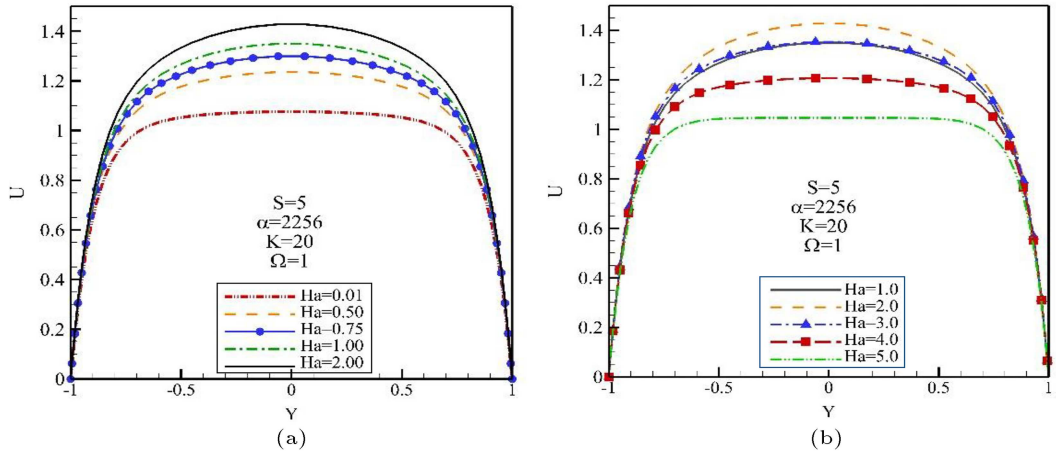

Figure 8. Developed velocity in microchannel cross- section under influence of $S = 5$, $\alpha = 2256$, and $\Omega = 1$, (a) $Ha \leq 1$, (b) $Ha \geq 1$.

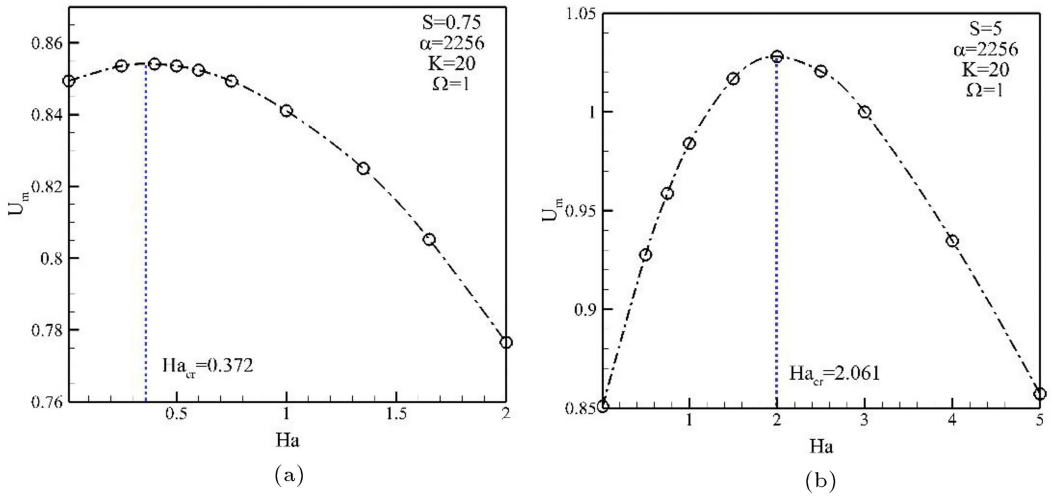

Figure 9. Average velocity variations with Hartmann number under influence of $\alpha = 2256$, $K = 20$, and $\Omega = 1$ for (a) $S = 0.75$ and (b) $S = 5$.

$(-\sigma u B_y^2)$, source term leads to apply a force to fluid in the same direction and flow rate augments. On the other hand, this velocity enhancement due to increase in magnetic field is not stable because by incrementing velocity, deterrent part augments, gradually. Finally, it could cause the deterrent part of this relation to become greater than driving part and consequently, a force opposite of the flow direction is applied to the fluid leading to a reduction in flow rate passing through the microchannel. For each value of Ha which the source term of Eq. (10) becomes maximum (critical Hartmann number), maximum flow velocity occurs.

While Figure 9 shows how Ha_{cr} in which the maximum flow rate and average velocity can be obtained in each dimensionless parameter of lateral electric field (S), Figure 10 shows the results of obtained Ha_{cr} and the maximum speed of flow versus S. Figure 10(a) indicates the variations of Ha_{cr} as a function of dimensionless parameter of lateral electric field (S) influenced by an axial electric field and pressure difference inside a 3-D microchannel with square a cross-section. As seen, for values of $S < 20$, by increasing the dimensionless parameter of lateral electric field, Ha_{cr} augments at a high rate. However, for the values of $S > 20$, the intensity of Ha_{cr} decreases, gradually.

Figure 10(b) represents maximum dimensionless average velocity as a function of S under influence of α and Ω. Maximum average flow velocity in the microchannel occurs at Ha_{cr} corresponding to each S, which the value of Ha_{cr} versus S is presented in Figure 10(a). By increasing S, maximum average velocity in microchannel and resultant passing flow rate enhances continually. The notable point is that in the constant axial electric field and the same conditions, by adding a lateral electric field with much lower power than the axial electric field and transverse magnetic field, the flow rate in the microchannel can be enhanced, and EOF can be amplified.

It should be mentioned that in Figure 10(a) and (b), for each value of S, there is a corresponding symbol

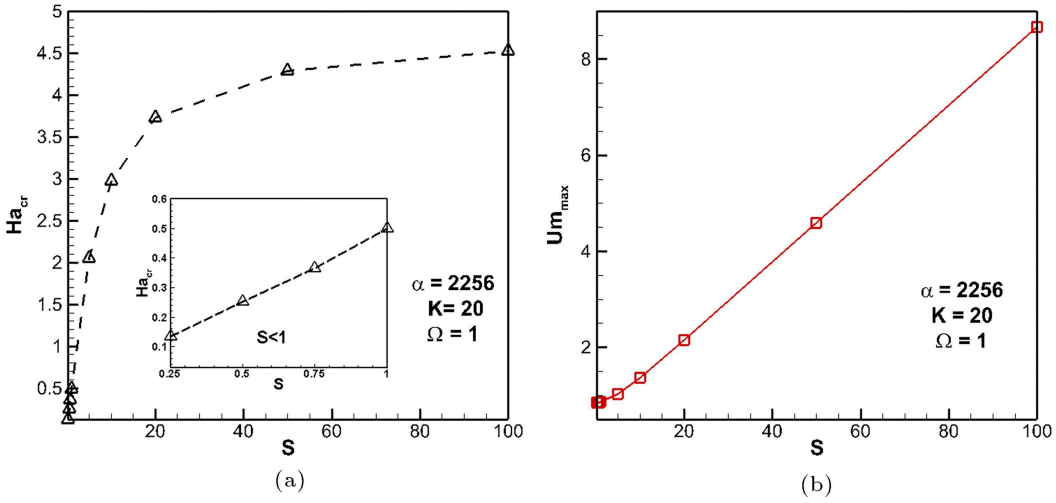

Figure 10. (a) Critical Hartmann number, (b) dimensionless maximum average velocity by means of dimensionless lateral electric field in 3D microchannel with square cross-section under influence of $\alpha = 2256$, $K = 20$, and $\Omega = 1$.

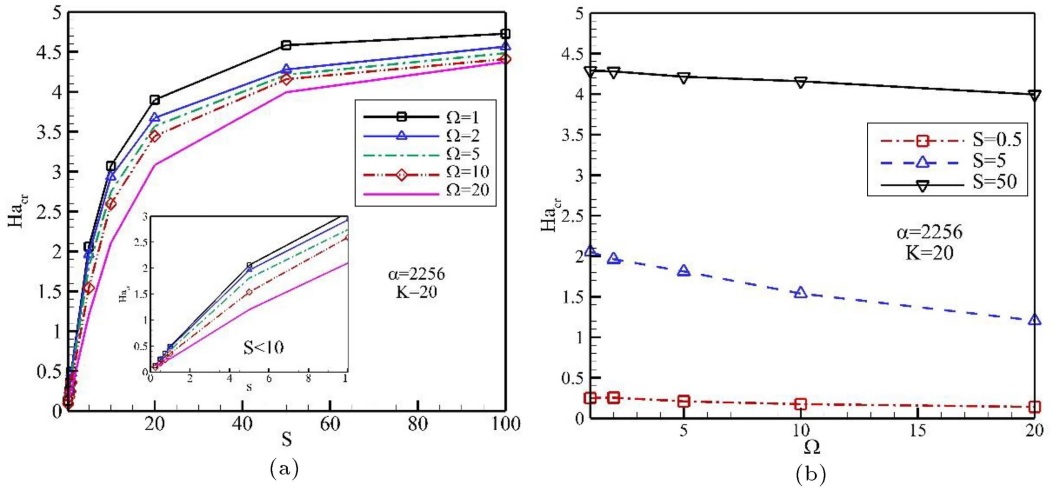

Figure 11. Critical Hartmann, number, (a) by means of dimensionless lateral electric field under influence of $\alpha = 2256$ and $K = 20$ in different values of Ω, (b) by means of dimensionless pressure gradient under influence of $\alpha = 2256$, and $K = 20$ in different values of S, in 3D microchannel with square cross-section.

in both figures. For instance, in Figure 10(b), at $S = 20$, $U_{m_{\max}} = 2.2$, and the corresponding Ha_{cr} value for this amount of S can be found in Figure 10(a), which is around 3.7.

In Figure 11(a) Ha_{cr} as a function of S is drawn for 5 different values of Ω. As seen, by increasing dimensionless parameter of pressure gradient (Ω) for each value of S, critical Hartmann number (Ha_{cr}) reduces. The reason for this could be that the rise in pressure gradient results in a reduction in the impact of the electroosmotic phenomenon on fluid motion in comparison to the movement caused by the axial pressure gradient. Figure 11(b) presents the variation of Ha_{cr} as a function of Ω for 3 lateral electric fields. By augmenting pressure difference along the microchannel, Ha_{cr} tends to decrease. As seen, for $S = 0.5$, the value of Ha_{cr} in $\Omega = 1$ and $\Omega = 20$ has a 44% difference, while the difference is about 7% for $S = 50$. Therefore, the effect of Ω on Ha_{cr} decreases by increasing S.

Figure 12 indicates the effect of dimensionless parameter of lateral electric field (S) on the Poiseuille number (Po) as a function of Ha for developed flow inside a microchannel with square cross-section influenced by axial electric field. As seen, in general, by enhancing Ha, Po augments. However, for different values of S, Po figure as the function of Ha shows a different behavior. Thus, for $S = 0$ and $S = 0.5$, Po continually increases by enhancing Ha. In $S = 0$, flow rate reduces by increasing Ha. Since, Po has reverse relation with the average velocity of flow $\left(Po \propto \frac{1}{U_m}\right)$, reduction of average velocity of flow leads to augmentation of the value of Po. In $S = 0.5$, Ha_{cr} has a negligible effect on the behavior of Po

because of its small amounts ($Ha_{cr} = 0.25$). For other electric fields' intensities, it has been seen that by increasing Ha, first Po tends to decrease and then tends to increase. Indeed, minimum value of Po in each lateral electric field, occurs approximately at the range of Ha_{cr} for that field. Because in this range, average velocity of flow is maximum and according to reverse relation between average velocity and Po, Poiseuille number decreases.

Figure 13 shows Ha_{cr} as a function of S in micro scale inside microchannel with the aspect ratios of $a =$ 2, 1, 0, 0.2, 0.5 with the same hydraulic diameter. The aspect ratio parameter is defined as the ratio of height to the width of channel section $\left(a = \frac{H}{W}\right)$ [39]. As seen, by converting square cross-section into two parallel plates (reduction of aspect ratio), the value of Ha_{cr} enhances for each S. This change is more sensitive for low aspect ratios. By changing the geometry of cross-section, because the hydraulic diameter is considered constant in each studied state, the dimension of microchannel and the contact surface of wall and fluid change.

In the constant pressure gradient and lower aspect ratios, friction and dissipation due to the contact of the fluid with the inner surface of the microchannel increase. This phenomenon is because of the contact between fluid and the higher surface of microchannel's wall. Therefore, the average velocity of flow passing through the microchannel reduces. By decreasing the flow velocity, second term or negative part of $-\sigma E_z B_y - \sigma u B_y^2$ term reduces in Eq. (10). Consequently, the stronger magnetic field or higher Ha is required to maximize flow rate or average velocity.

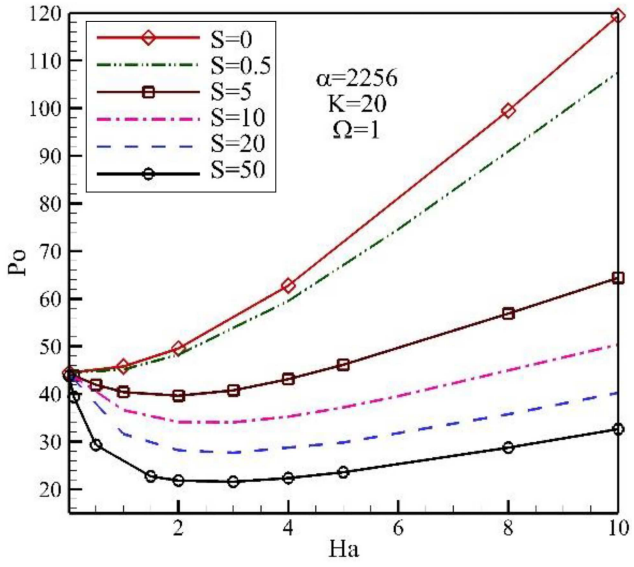

Figure 12. Effect of lateral electric field on graph of Poiseuille number by means of Ha under influence of $\alpha = 2256$, $K = 20$, and $\Omega = 1$.

6.2. Heat transfer analysis

Figure 14 indicates dimensionless temperature profile of developed EOF influenced by lateral electric field and transverse magnetic field and pressure gradient. In the absence of lateral electric field for the values of $Ha \leq 1$, the enhancement of magnetic field leads to a slight increase in maximum dimensionless temperature. However, for values of $Ha \leq 1$, the augmentation of Hartmann number (Ha) causes considerable increment of maximum dimensionless temperature profile and also, becomes wider. In the vicinity of surface in higher

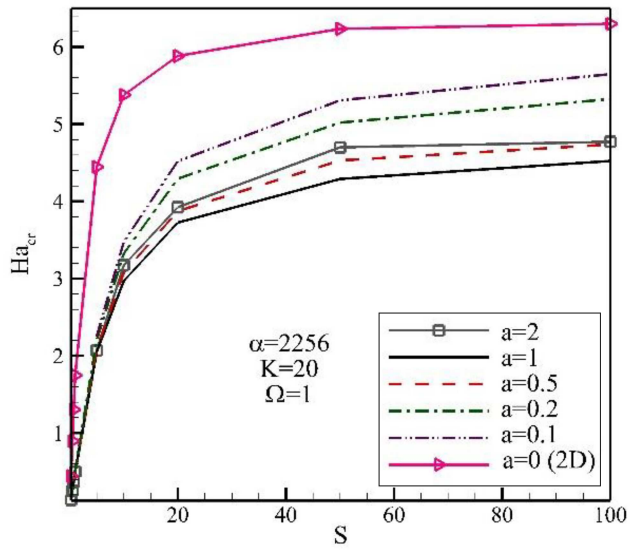

Figure 13. Critical Hartmann number by means of dimensionless lateral electric field under influence of $\alpha = 2256$, $K = 20$, and $\Omega = 1$ in different values of aspect ratio.

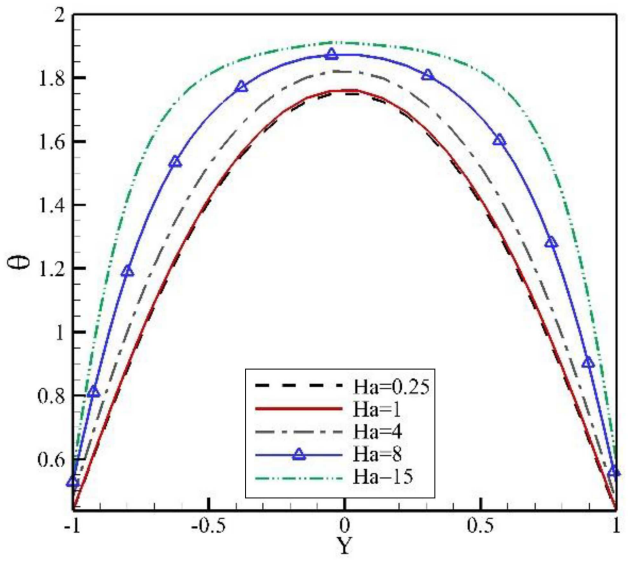

Figure 14. Fully developed and dimensionless temperature profile in microchannel with square cross-section on $Z = 0$ line without applying lateral electric field.

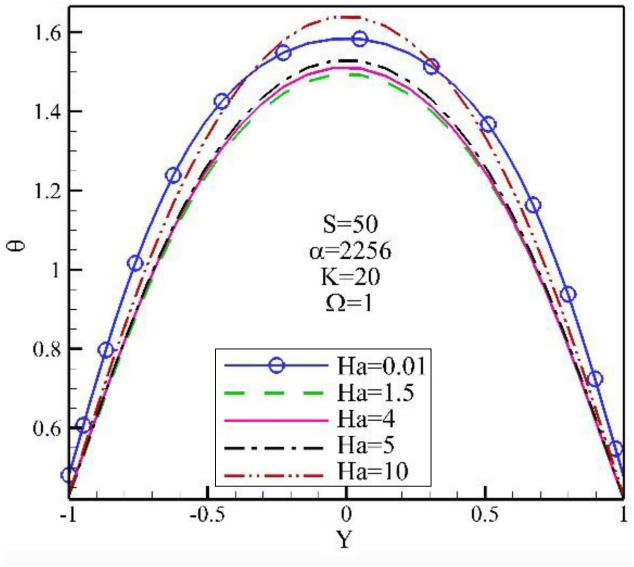

Figure 15. Fully developed and dimensionless temperature distribution in microchannel with square cross-section on $Z = 0$ line in presence of lateral electric field.

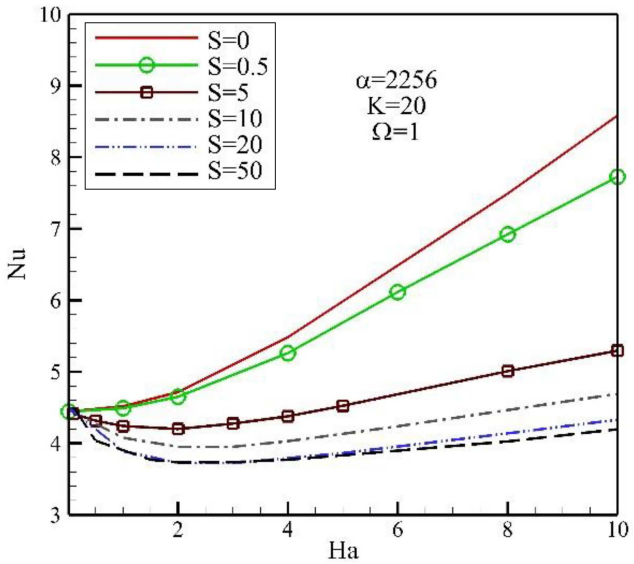

Figure 16. Effect of applying lateral electric field on Nusselt number figure by means of Hartmann number under influence of $\alpha = 2256$, $K = 20$, and $\Omega = 1$.

Ha, the increase in temperature gradient means the enhancement of convective heat transfer coefficient which means reduction in surface temperature difference and average temperature of fluid, according to the constant heat flux condition on the surface.

Figure 15 shows dimensionless temperature profile of developed EOF under influence of various values of transverse magnetic field in the presence of lateral electric field. In this figure flow velocity increased due to the interaction of driving and deterrent forces caused by the electromagnetic field applied to the channel. Under influence of this condition, local temperature of fluid reduces causing the augmentation of the value of $T - T_w$. Also, the increase in average velocity leads to a reduction in average temperature in each cross-section. Therefore, the value of $T_m - T_w$ increases in the denominator of the dimensionless temperature θ. However, the increment of numerator of θ is lower than the increase in its denominator. Consequently, by enhancing the value of Ha, the value of dimensionless temperature decreases in the cross-section. By passing from Ha_{cr}, Hartmann number increment leads to decrease in the average velocity of flow and heat transfer, because the movement of fluid mass reduces, and the value of heat transfer diffusion rate enhances. Consequently, the value of dimensionless temperature increases in the cross-section.

Figure 16 reveals the effect of lateral electric field on Nusselt number (Nu) in electroosmotic developed flow for each Ha inside a microchannel with square cross-section influenced by distinct lateral electric field (S) and pressure gradient. For $S = 0$ and $S = 0.5$, by increasing Ha, Nu has incremental trend and enhances in all values of Ha. According to constant heat flux boundary condition ($q'' = h(T_w - T_m)$), Ha enhancement leads to reduction in $T_w - T_m$ and consequently, increase in convective heat transfer coefficient, gradually. In the stronger lateral electric field ($S \geq 5$), Nu becomes minimum in a specific Ha called critical Hartmann number ($Ha_{cr,T}$). By comparing around the Nusselt number minimization, it reveals that $Ha_{cr,T}$ is greater than Ha_{cr} for $S = 5$, 10 and is lower than Ha_{cr} for $S = 20$, 50.

7. Conclusion

This research studied the electroosmotic flow of an electrolyte solution under the influence of a lateral electric field and a transverse magnetic field inside a microchannel. The purpose of this paper was to do a three-dimensional simulation which is necessary for practical applications, and to observe the flow physics and investigate the effect of different parameters on it. For modeling the electric potential in the electrolyte at the vicinity of walls, the Poisson-Boltzmann equation is used with the Debye-Hückel approximation. The governing equations of the flow are solved by using a numerical code and finite volume method by utilizing SIMPLEC algorithm. Also, the properties of the fluid are proposed constant.

Although effective parameters on flow are mainly implemented for microchannel with a square cross-section, the effect of the aspect ratio of channel cross-section is investigated on the microchannel flow. In addition, energy equation is solved by considering constant heat flux and Joule heating. The following conclusions are drawn from the results of this research:

- A secondary flow is created with a specific pattern at

the microchannel cross-section due to simultaneous application of lateral electric field and transverse magnetic field on electroosmotic flow;

- By increasing the rate of the lateral electric field, the value of the critical Hartmann number enhances which flow rate becomes maximum. However, from a specific value of the lateral electric field, the enhancement rate of the critical Hartmann number decreases. In case of the lateral electric field parameter of $S = 0.5$, Ha_{cr} has 44% difference Between $\Omega = 1$ and $\Omega = 20$;
- The geometry of the microchannel cross-section affects the value of the critical Hartmann number. So that by changing aspect ratio from rectangular cross-section to squared, the value of Ha_{cr} augments, in this augmentation is more sensitive to lower aspect ratios.

In higher lateral electric fields, first, the gradual enhancement of magnetic field leads to reduced Nusselt number of development flow. However, after a specific value of the Hartmann number, the augmentation of the magnetic field leads to the enhancement of the Nusselt number. In the lower values of lateral electric fields, by increasing Hartmann number, Nusselt number enhances steadily. This flow and heat transfer problem can be employed in many areas such as bioengineering and is particularly useful in the manufacture of pharmaceutical microfluidic devices and flow delivery systems.

Nomenclature

b	Induced magnetic field, Vsm^{-2}
B	Applied externally magnetic field strength, Vsm^{-2}
B_y	Applied magnetic field in y-direction, Vsm^{-2}
D_H	Hydraulic diameter, m
e	Charge of an electron, C
E	Externally applied electric field strength, Vm^{-1}
E_x	Externally applied electric field in x-direction, Vm^{-1}
E_z	Externally applied electric field in z-direction, Vm^{-1}
F	Body force vector, N
F_{EK}	Electrokinetic body force, N
H	Microchannel half height, m
Ha	Hartmann number
Ha_{cr}	Critical Hartmann number
$Ha_{cr,T}$	Thermal critical Hartmann number
J	Induced electric current density, Am^{-1}
K_B	Boltzmann constant, JK^{-1}
L	Micro channel length, m
N	Ionic number concentration, m^{-3}
n_0	Bulk concentration of the ions, m^{-3}
P	Pressure, Nm^{-2}
Re_m	Magnetic Reynolds number
S	Dimensionless electric field in z-direction
T	Absolute temperature, K
u	Flow velocity in x-direction, ms^{-1}
U	Dimensionless flow velocity in x-direction
U_{av}	Dimensionless average flow velocity
u_{av}	Average flow velocity in x-direction, ms^{-1}
u_{HS}	Helmholtz-Smoluchowski velocity, ms^{-1}
$u_{\max}$	Maximum flow velocity in x-direction, ms^{-1}
$U_{\max}$	Dimensionless maximum flow velocity
v	Flow velocity in y-direction, ms^{-1}
V	Flow velocity vector, ms^{-1}
w	Flow velocity in z-direction, ms^{-1}
Y	Dimensionless height
z_i	Valency of ith ionic species
α	Dimensionless electric field in x-direction
ε	Relative permittivity of the medium
ε_0	Permittivity of free space, $\mathrm{CV}^{-1}\mathrm{m}^{-1}$
ς	Wall zeta potential, V
κ	Debye-Hückel parameter, m^{-1}
K	Dimensionless Debye-Hückel parameter
λ_D	Debye length, m
μ	Viscosity of the electrolyte, $\mathrm{kgm}^{-1}\mathrm{s}^{-1}$
ρ_e	Electric charge density, Cm^{-3}
ρ_f	Electrolyte density, kgm^{-3}
σ	Electric conductivity of the electrolyte, Sm^{-1}
ϕ	Electrostatic potential, V
ψ	Electrical double layer potential, V
Ω	Dimensionless pressure gradient

References

1. Gad-El-Hak, M. "The fluid mechanics of microdevices-the freeman scholar lecture", *Journal of Fluids Engineering, Transactions of the ASME*, **121**(1), pp. 5–33 (1999). DOI: 10.1115/1.2822013
2. Probstein, R.F., *Physicochemical Hydrodynamics: An Introduction*, John Wiley and Sons (2005). DOI: 10.1002/9780471725121

3. Manz, A., Graber, N., and Widmer, H.M. "Miniaturized total chemical analysis systems: A novel concept for chemical sensing", *Sens Actuators B Chem*, **1**(1–6), pp. 244–248 (1990). DOI: 10.1016/0925-4005(90)80209-I

4. Jang, J. and Lee, S.S. "Theoretical and experimental study of MHD (magneto hydrodynamic) micro pump", *Sens Actuators A Phys*, **80**(1), pp. 84–89 (2000). DOI: 10.1016/S0924-4247(99)00302-7

5. Laser, D.J. and Santiago, J.G. "A review of micropumps", *Journal of Micromechanics and Microengineering*, **14**(6), pp. R35–R64 (2004). DOI: 10.1088/0960-1317/14/6/R01

6. Nguyen, N.T., Huang, X., and Chuan, T.K. "MEMS-micropumps: A review", *Journal of Fluids Engineering, Transactions of the ASME*, **124**(2), pp. 384–392 (2002). DOI: 10.1115/1.1459075

7. Karniadakis, G., Beskok, A., and Aluru, N., *Microflows and Nanoflows: Fundamentals and Simulation*, Springer Science and Business Media (2006). DOI: 10.1007/0-387-28676-4

8. Das, S., Chakraborty, S., and Mitra, S.K. "Magnetohydrodynamics in narrow fluidic channels in presence of spatially non-uniform magnetic fields: Framework for combined magnetohydrodynamic and magnetophoretic particle transport", *Microfluid Nanofluidics*, **13**(5), pp. 799–807 (2012). DOI: 10.1007/s10404-012-1001-z

9. Sarkar, S., Ganguly, S., and Dutta, P. "Thermofluidic characteristics of combined electroosmotic and pressure driven flows in narrow confinements in presence of spatially non-uniform magnetic field", *Int J Heat Mass Transf*, **104**, pp. 1325–1340 (2017). DOI: 10.1016/j.ijheatmasstransfer.2016.09.072

10. Wang, P.J., Chang, C.Y., and Chang, M.L. "Simulation of two-dimensional fully developed laminar flow for a magneto-hydrodynamic (MHD) pump", *Biosens Bioelectron*, pp. 115–121 (2004). DOI: 10.1016/j.bios.2003.10.018

11. Chakraborty, S. and Paul, D. "Microchannel flow control through a combined electromagnetohydrodynamic transport", *J Phys D Appl Phys*, **39**, p. 5364 (2006). DOI: 10.1088/0022-3727/39/24/038

12. Duwairi, H. and Abdullah, M. "Thermal and flow analysis of a magneto-hydrodynamic micropump", *Microsystem Technologies*, **13**(1), pp. 33–39 (2007). DOI: 10.1007/s00542-006-0258-0

13. Chakraborty, R., Dey, R., and Chakraborty, S. "Thermal characteristics of electromagnetohydrodynamic flows in narrow channels with viscous dissipation and Joule heating under constant wall heat flux", *Int J Heat Mass Transf*, **67**, pp. 1151–1162 (2013). DOI: 10.1016/j.ijheatmasstransfer.2013.08.099

14. Escandón, J., Santiago, F., Bautista, O., et al. "Hydrodynamics and thermal analysis of a mixed electromagnetohydrodynamic- pressure driven flow for Phan-Thien-Tanner fluids in a microchannel", *International Journal of Thermal Sciences*, **86**, pp. 246–257 (2014). DOI: 10.1016/j.ijthermalsci.2014.07.009

15. Kiyasatfar, M. and Pourmahmoud, N. "Laminar MHD flow and heat transfer of power-law fluids in square microchannels", *International Journal of Thermal Sciences*, **99**, pp. 26–35 (2016). DOI: 10.1016/j.ijthermalsci.2015.07.031

16. Wang, L., Jian, Y., Liu, Q., et al. "Electromagneto-hydrodynamic flow and heat transfer of third grade fluids between two micro-parallel plates", *Colloids Surf A Physicochem Eng Asp*, **494**(494), pp. 87–94 (2016). DOI: 10.1016/j.colsurfa.2016.01.006

17. Qi, C. and Wu, C. "Electromagnetohydrodynamic flow in a rectangular microchannel", *Sens Actuators B Chem*, **263**, pp. 643–660 (2018). DOI: 10.1016/j.snb.2018.02.107

18. Yang, C., Jian, Y., Xie, Z., et al. "Heat transfer characteristics of magneto hydrodynamic electroosmotic flow in a rectangular microchannel", *European Journal of Mechanics-B/Fluids*, **74**, pp. 180–190 (2019). DOI: 10.1016/j.euromechflu.2018.11.015

19. Moradmand, A., Saghafian, M., and Mofrad, B. "Electroosmotic pressure-driven flow through a slit microchannel with electric and magnetic transverse field", *Journal of Applied Fluid Mechanics*, **12**, pp. 961–969 (2019). DOI: 10.29252/jafm.12.03.28816

20. Yang, C.-H. and Jian, Y.-J. "Effect of patterned hydrodynamic slip on electromagnetohydrodynamic flow in parallel plate microchannel", *Chinese Physics B*, **29**(11), p. 114101 (2020). DOI: 10.1088/1674-1056/abab71

21. Deng, S., Xiao, T., and Wu, S. "Two-layer combined electroosmotic and pressure-driven flow of power-law fluids in a circular microcapillary", *Colloids Surf A Physicochem Eng Asp*, **610**, p. 125727 (2021). DOI: 10.1016/j.colsurfa.2020.125727

22. Ge, Y., He, Q., Lin, Y., et al. "Multi-objective optimization of a mini-channel heat sink with non-uniform fins using genetic algorithm in coupling with CFD models", *Appl Therm Eng*, **207**, p. 118127 (2022). DOI: 10.1016/j.applthermaleng.2022.118127

23. Wang, G., Qian, N., and Ding, G. "Heat transfer enhancement in microchannel heat sink with bidirectional rib", *Int J Heat Mass Transf*, **136**, pp. 597–609 (2019). DOI: 10.1016/j.ijheatmasstransfer.2019.02.018

24. Biswas, N., Mondal, M.K., Mandal, D.K., et al. "A narrative loom of hybrid nanofluid-filled wavy walled tilted porous enclosure imposing a partially active magnetic field", *Int J Mech Sci*, **217**, p. 107028 (2022). DOI: 10.1016/j.ijmecsci.2021.107028

25. Mandal, D.K., Biswas, N., Manna, N.K., et al. "Thermo-fluidic transport process in a novel M-shaped

cavity packed with non-Darcian porous medium and hybrid nanofluid: Application of artificial neural network (ANN)", *Physics of Fluids*, **34**(3), p. 033608 (2022). DOI: 10.1063/5.0082942

26. Datta, A., Debbarma, D., Biswas, N., et al. "The Role of Flow Structures on the Thermal Performance of Microchannels With Wall Features", *J Therm Sci Eng Appl*, **13**(2), p. 021019 (2020). DOI: 10.1115/1.4047709
27. Amit, K., Datta, A., Biswas, N., et al. "Designing of microsink to maximize the thermal performance and minimize the Entropy generation with the role of flow structures", *Int J Heat Mass Transf*, **176**, p. 121421 (2021). DOI: 10.1016/j.ijheatmasstransfer.2021.121421
28. Biswas, N., Chamkha, A.J., and Manna, N.K. "Energy-saving method of heat transfer enhancement during magneto-thermal convection in typical thermal cavities adopting aspiration", *SN Appl Sci*, **2**(11), p. 1911 (2020). DOI: 10.1007/s42452-020-03634-w
29. Alharbi, K.A.M., Khan, Z., Zuhra, S., et al. "Numerical study of the electro magneto hydro dynamic bio convection flow of micro polar nano fluid through a stretching sheet with thermal radiation and stratification", *ACS Omega*, **7**(47), pp. 42733–42751 (2022). DOI: 10.1021/acsomega.2c04145
30. Ciocanel, C. and Islam, N. "Integrated Electro-Magnetochydrodynamic Micropumps and Methods for Pumping Fluids", *U.S. Patent US-8480377-B2* (July 9, 2013).
31. Alipanah, M., Hafttananian, M., Hedayati, N., et al. "Microfluidic on-demand particle separation using induced charged electroosmotic flow and magnetic field", *J Magn Magn Mater*, **537**, p. 168156 (2021). DOI: 10.1016/j.jmmm.2021.168156
32. Masliyah, J.H. and Bhattacharjee, S., *Electrokinetic and Colloid Transport Phenomena*, Wiley-Interscience (2006). DOI: 10.1002/0471799742
33. Davidson, P.A. "An introduction to magnetohydrodynamics" (2002). DOI: 10.1017/9781316672853
34. Müller, U. and Bühler, L., *Magneto Fluid Dynamics in Channels and Containers*, Springer Berlin Heidelberg, Berlin, Heidelberg (2001). DOI: 10.1115/1.1445331
35. Mirbozorgi, S.A., Niazmand, H., and Renksizbulut, M. "Electro-osmotic flow in reservoir-connected flat microchannel with non-uniform zeta potential", *Journal of Fluids Engineering, Transactions of the ASME*, **128**(6), pp. 1133–1143 (2006). DOI: 10.1115/1.2353261
36. Deng, S.Y., Jian, Y.J., Bi, Y.H., et al. "Unsteady electroosmotic flow of power-law fluid in a rectangular microchannel", *Mech Res Commun*, **39**(1), pp. 9–14 (2012). DOI: 10.1016/j.mechrescom.2011.09.003
37. Lim, J., Lanni, C., Evarts, E.R., et al. "Magnetophoresis of nanoparticles", *ACS Nano*, **5**(1), pp. 217–226 (2011). DOI: 10.1021/nn102383s
38. Nguyen, N.-T. "Micro-magnetofluidics: interactions between magnetism and fluid flow on the microscale", *Microfluid Nanofluidics*, **12**(1–4), pp. 1–16 (2012). DOI: 10.1007/s10404-011-0903-5
39. Chen, X. and Hu, Z. "Study aspect ratio of microchannel on different polymer substrates with CO_2 laser and hot bonding for microfluidic chip", *AIP Adv*, **8**(1), p. 015116 (2018). DOI: 10.1063/1.5012772

Biographies

Mohsen Saghafian is an Associate Professor in the Department of Mechanical Engineering at Isfahan University of Technology, Isfahan, Iran, specializing in CFD, Fluid Mechanics, Heat and Mass Transfer, MHD, EHD, Microfluidics, Numerical techniques, and Turbulence. His research focuses on various topics, such as particle separation in microfluidic devices, acoustic radiation force on biological cells, blood flow in stenosed arteries, tumor modeling, fluid flow and heat transfer in microchannels under electric and magnetic fields, and convection heat transfer in nonhomogeneous nanofluids.

Hossein Seyedzadeh received his MSc degree in Mechanical Engineering from Isfahan University of Technology, Isfahan, Iran, in 2020. He is now a PhD student and research assistant in the department of Civil Engineering at Stony Brook University, NY, USA. His research interests are CFD simulation of Energy, Environmental and Biological Fluid Dynamics. He is also experienced in the MHD and EHD flows.

Abolfazl Moradmand received his BSc degree in mechanical engineering from Yazd University, Yazd, Iran, in 2014 and his MSc degree in mechanical engineering from Isfahan University of Technology, Isfahan, Iran, in 2018. His research interests include Electro-Hydrodynamic flows and Microchannels.